Prediction of robust two-dimensional topological insulators based on Ge/Si nanotechnology

Christophe Delerue

Prediction of robust two-dimensional topological insulators based on Ge/Si nanotechnology

Christophe Delerue*
IEMN - Département ISEN, UMR CNRS 8520, Lille, France
(Received 7 April 2014; revised manuscript received 12 August 2014; published 22 August 2014)

Atomistic tight-binding calculations show that two-dimensional topological insulators can be obtained using Ge or Ge/Si nanotechnologies. The strong quantum confinement is used to open energy gaps in the valence band of artificial graphene made of Ge. These gaps are topologically nontrivial due to the combination of the honeycomb nanogeometry and the spin-orbit coupling. Gap widths above 10 meV can be obtained using realistic structures. With light effective masses, a strong spin-orbit coupling, and a high compatibility with microelectronic processes, Ge is an excellent substrate for the fabrication of spintronic devices based on topological insulator states.

DOI: 10.1103/PhysRevB.90.075424 PACS number(s): 71.70.Ej, 72.25.Mk, 75.76.+j

I. INTRODUCTION

Topological insulators (TIs) are of considerable interest for their potential applications in spintronics and quantum computation because their boundaries are characterized by topologically protected gap states with helical spin polarization [1,2]. These edge states carry dissipationless spin currents, leading in two-dimensional (2D) systems to the quantum spin Hall (QSH) effect which is realized by the spin-orbit (SO) coupling instead of a magnetic field in the QH effect. The QSH effect was initially predicted for graphene [3] but the SO coupling is too small to give measurable effects [4]. Soon after, the prediction of the QSH effect in HgTe quantum wells [5] led to the first observation of a 2D TI state of matter [6]. Nowadays, many other 2D TIs are investigated, such as thin films of Bi [7], Sn [8,9], or $Ge(Bi_xSb_{1-x})_2Te_4$ [10], silicene and its Ge analog [11], GaAs/Ge/GaAs quantum wells [12], and inverted InAs/GaSb quantum wells [13,14]. It was also shown that 2D TIs could be made from semiconductors on which a potential with hexagonal symmetry is superimposed [15]. Very recently, TI properties have been predicted in honeycomb superlattices of CdSe nanocrystals [16]. However, the applications in spintronics of 2D TIs are still being awaited even if sophisticated devices have been recently made from HgTe quantum wells [17]. One likely reason for the small number of applications is the lack of 2D TIs compatible with standard Si microelectronic technology which could foster the fabrication of devices.

The present work demonstrates that 2D TIs with nontrivial gap widths above 10 meV can be made using Ge or Ge/Si nanotechnologies. The strategy is to realize artificial graphene [18,19] in which the carbon atoms are replaced by semiconductor materials with strong SO coupling [15,16]. Ge is a material of choice with a SO splitting of 296 meV at the top of its valence band. I present atomistic tight-binding calculations of the electronic structure of thin Ge and Ge/Si sheets with honeycomb nanogeometry. In the case of Ge/Si materials, the effects of strains on the electronic structure are included. It is shown that the valence band of these superlattices is composed of minibands and the gap between the two highest minibands is topologically nontrivial in a wide range of geometrical configurations. The presence of a second nontrivial gap is also possible depending on geometrical factors. The topological properties are assessed by calculations of the Z_2 topological invariant (hereafter D) [3,20]. This is confirmed by the presence of helical edge states in ribbons built from the superlattices. In a context where Ge and Ge/Si technologies receive growing attention [21], the present work demonstrates their interest for nonconventional applications based on TI properties.

II. METHODOLOGY

A. Geometry of the superlattices

Two types of honeycomb superlattices have been studied (Fig. 1). The first one is a direct analog of graphene in which each carbon atom is replaced by a spherical Ge nanocrystal. The diameter d of the spheres is equal to the honeycomb lattice spacing a; i.e., neighbor spheres are tangential. Each pair of neighbors is connected by a horizontal cylinder of Ge whose diameter is a fraction of the sphere diameter (30%–100%). All Ge atoms contained in the spheres and the cylinders are included in the structure and are positioned at the same atomic sites as in bulk Ge. Depending on the size, it results in slightly faceted shapes. The cylinders are barely visible in Fig. 1(a) because neighbor spheres are tangential but these cylinders play an important role by determining the coupling between nanocrystals. The free surfaces are passivated by hydrogen (not shown). We will see in the following that these structures exhibit very interesting 2D TI properties.

Inspired by this model system, I consider a second type of superlattice which could be fabricated using microelectronic Ge/Si technology including nanoscale lithography. These superlattices can be seen as assemblies of parallel Ge cylinders organized on a honeycomb lattice [Fig. 1(b)]. The axes of the cylinders are perpendicular to the 2D lattice. The space between the cylinders is filled with Si atoms. The length of the vertical cylinders determines the thickness t of the active material. A small passivating layer of Si is also added on each side of the sheet (typically 0.6 nm). The Ge components of the superlattices are thus fully surrounded by Si. The atomic structure of the supercells is relaxed using Keating's valence force field model [22] as described in Ref. [23] to account for the important lattice mismatch between Si and Ge (4%).

*christophe.delerue@isen.fr

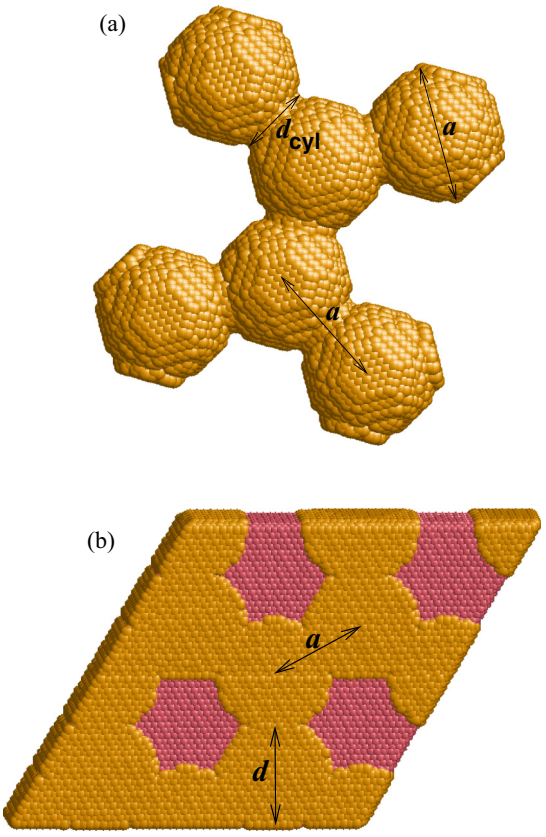

FIG. 1. (Color online) Top view of honeycomb superlattices considered in this work (Ge atoms in yellow, Si ones in pink, a is the lattice spacing). (a) First type: Assembly of Ge spheres (diameter $d = a = 4.4$ nm) connected by horizontal Ge cylinders (diameter $d_{cyl} = 0.5d$). (b) Second type: Assembly of vertical Ge cylinders ($d = 1.1a = 6.6$ nm, length = sheet thickness $t = 4.8$ nm), the space between them being filled by Si. The bottom and top sides of the sheet are covered by approximately 0.6 nm of Si (not shown for clarity). For both types of superlattices, the vertical axis corresponds to the $\langle 111 \rangle$ axis of the zinc-blende crystal. The in-plane orthogonal $\langle \bar{1}10 \rangle$ and $\langle 1\bar{1}0 \rangle$ axes sustain the superlattice vectors.

The description of strain effects is required to predict band structures with accuracy. However, the nontrivial topology of the bands is not determined by these effects.

B. Tight-binding calculations

The electronic structure of the two types of superlattices is computed using an atomistic tight-binding method. Each Ge or Si atom is described by a double set of $sp^3d^5s^*$ atomic orbitals including the spin degree of freedom. The orbitals are assumed to be orthogonal and the matrix elements between two orbitals are restricted to first nearest-neighbor interactions. The Hamiltonian matrix is calculated using the tight-binding parameters derived in Ref. [23] to describe electronic bands, effective masses, and deformation potentials of bulk Si and Ge. There is no free parameter in the calculations. As usual in tight binding [24], the SO coupling is described by intra-atomic Hamiltonian matrix elements in the p sector [23,25].

Due to the nanoscale geometry, the unit cell of the superlattices contains a large number of atoms. For example, there are 29 744 Ge (Si) atoms in the structure of Fig. 1(b), meaning that its valence band is in fact composed of $4 \times 29\,744$ filled bands (minibands). The nanogeometry induces periodic scattering of the electronic waves, opening gaps at the center and at the edges of the superlattice Brillouin zone [16,26,27], but these gaps are only visible near the top of the valence bands or the bottom of the conduction bands, where the effects of the confinement are the stronger. In practice, only the minibands in these regions close to valence/conduction band edges are calculated using the numerical methods described in Ref. [28].

The Z_2 topological invariant for the bands of interest is calculated following the methodology proposed in Ref. [29]. D is given by a sum of terms calculated on a regular lattice in the Brillouin zone. In any case, I have checked that the results are converged for a mesh denser than 101×101 k vectors. This approach works even for systems without inversion symmetry, which is the case for the superlattices investigated here. Experimentally, the realization of structures presenting inversion symmetry is unlikely since it would require control of the geometry at the atomic level.

In the present work, only the results concerning the valence bands of the superlattices are presented since the conduction bands which are weakly influenced by the SO coupling have a trivial topology. In the case of Ge/Si superlattices, the Si component forms a large energy barrier (0.68 eV) for the holes which are therefore localized in the Ge component. By convention, in the following, the zero of energy is fixed at the top of the valence band of bulk Si.

III. SUPERLATTICES OF Ge NANOCRYSTALS

A. Band structure and topological properties

Typical results for honeycomb superlattices of Ge nanocrystals are shown in Fig. 2. As discussed above, the electronic structure is characterized by multiple minibands but only the highest valence minibands are presented [Fig. 2(a)]. The minimum of the conduction bands (not shown) is at 1.70 eV, the quantum confinement opening a large energy gap of 1.18 eV. The two highest valence minibands, denoted band 1 and band 2 in Fig. 2(a), are in fact doublets of quasidegenerate bands. The origin of this almost invisible splitting within each doublet will be discussed in Sec. III B. The band 1 is characterized by a unitary Z_2 topological invariant, meaning that the minigap below (hereafter first gap) is topologically nontrivial. The gap (hereafter second gap) between bands 2 and 3 of Fig. 2(a) is also nontrivial as the Z_2 topological invariant for the ensemble of bands 1–2 is once again unitary.

The nontrivial character of the gaps between bands 1, 2, and 3 is confirmed by Fig. 2(b) showing the band structure of armchair and zigzag ribbons made from the same superlattice. The wave vector k is along the direction of the ribbon. The manifolds of bands situated in the energy regions corresponding to bands 1, 2, and 3 of the 2D superlattice [Fig. 2(a)] basically come from the folding of the 2D bands into the 1D Brillouin zone. In the gaps, there are topologically protected edge states, as found for graphene with SO coupling [3,30]. The wave functions corresponding to these states are localized on the nanocrystals at the edges (Fig. 3) and their spin component is mainly oriented perpendicular to the lattice

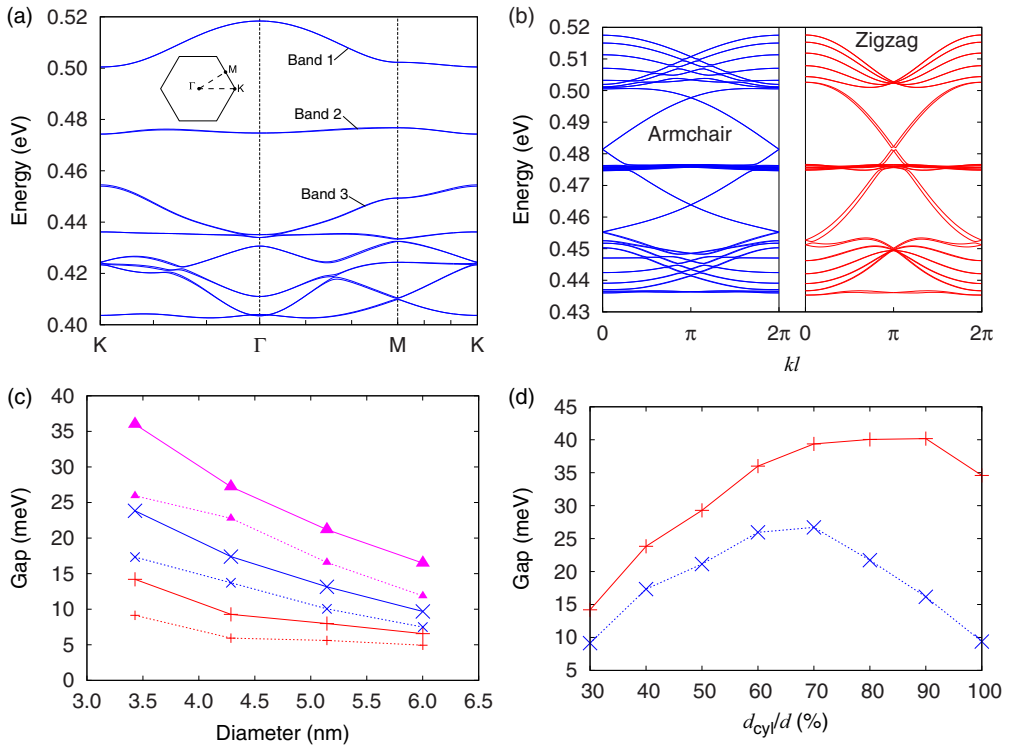

FIG. 2. (Color online) Results for honeycomb superlattices of spherical Ge nanocrystals. (a) Highest valence bands for the superlattice described in Fig. 1(a) versus k along the path shown in the inset. (b) Highest valence bands in a ribbon made from the same superlattice (left, blue: 20 nanocrystals per unit cell, armchair edge geometry; right, red: 12 nanocrystals per unit cell, zigzag edge). l is the length of the supercell. (c) Solid lines: Width of the first gap between bands 1 and 2 as a function of the nanocrystal diameter d for $d_{cyl} = 0.3d$ (+, red), $0.4d$ (×, blue), $0.6d$ (▲, magenta). Dotted lines: Same for the second gap between bands 2 and 3. (d) Width of the first (red solid line, +) and second (blue dotted line, ×) gap versus d_{cyl}/d.

(>97%), the direction of the spin being inverted for motions in opposite directions ($k \rightarrow -k$) [16].

The small splitting between the edge states in the case of the zigzag ribbon [Fig. 2(b)] is induced by a small anisotropy between the left and right sides of the ribbon (the armchair ribbon is built symmetric). This anisotropy was introduced on purpose; atoms were removed from nanocrystals at one side of the ribbon. This shows that edge states are obtained whatever the situation, thanks to their topological protection. The wave function shown in Fig. 3 is localized on one side of the ribbon due to the asymmetry. In the symmetric case (not shown), it is equally shared between left and right sides (see also Ref. [16]).

Figure 2(c) shows that a width of the first gap above 10 meV can be obtained for realistic sizes. The width of second gap is slightly smaller. When the diameter d_{cyl} of the connecting cylinders is changed, the width of the first gap saturates at a maximum for $d_{cyl}/d \approx 70\%$–90% [Fig. 2(d)].

B. Origin of the nontrivial topology

In bulk Ge, the electronic bands at the top of the valence band are derived from Bloch states of Ge p orbitals. They form heavy-hole, light-hole, and split-off bands, the splitting between the latter and the two others being induced by the SO coupling. In superlattices, the nanogeometry induces complex

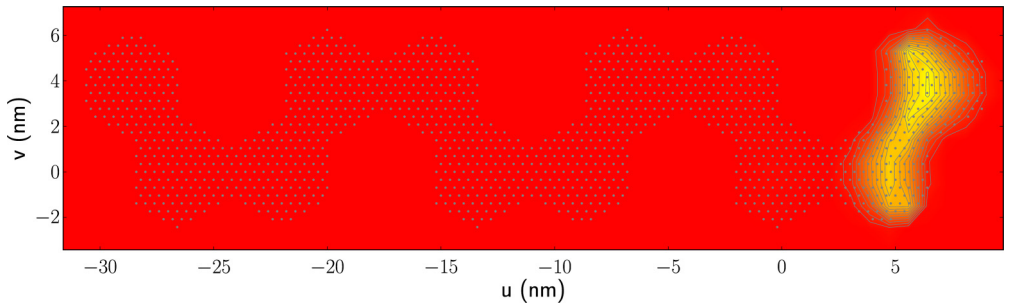

FIG. 3. (Color online) 2D plots of the wave function of a edge state calculated at $k = 0.4 \times 2\pi/l$ for the zigzag ribbon considered in Fig. 2(b) (energy of the state equaling approximately 0.49 eV). The plot is restricted to a single unit cell of the ribbon. The vertical axis corresponds to the direction of the ribbon. The white dots indicate the atoms.

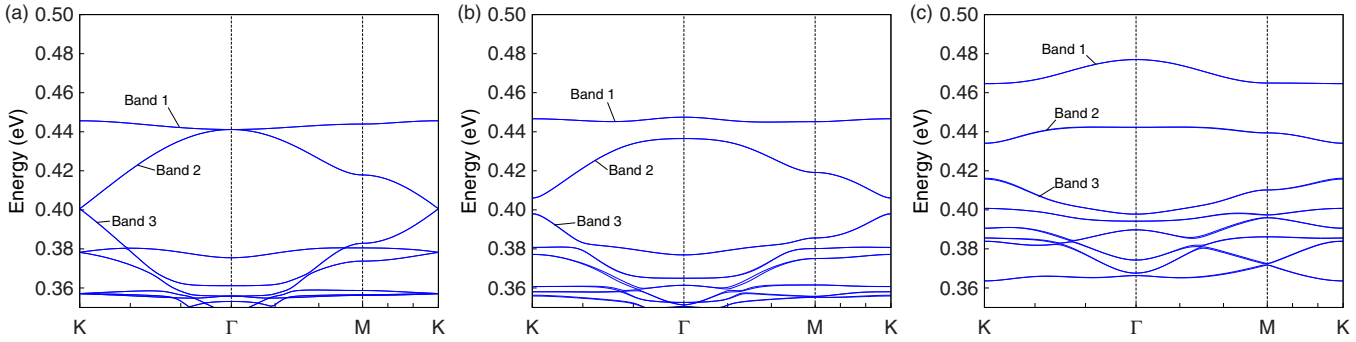

FIG. 4. (Color online) Superlattice of Ge nanocrystals described in Fig. 1(a): Highest valence bands calculated for a varying percentage of the nominal SO coupling on the Ge atoms: 0% (a), 10% (b), 50% (c), 100% [Fig. 2(a)].

mixing between these bands. In order to understand the origin of the nontrivial gaps in a simple manner, it is instructive to look at the variations of the band structure of superlattices when the SO coupling on each Ge atom is tuned between zero and its nominal value (its value derived for bulk Ge). In the following, we consider successively the situations of vanishing (Sec. III B 1), weak (Sec. III B 2), or strong (Sec. III B 3) SO coupling. Results are discussed in Sec. III B 4.

1. Superlattice band structure without SO coupling

In the absence of SO coupling [Fig. 4(a)], there is no more gap between the minibands. There are several Dirac cones at the K points. The highest band (1) is almost totally flat and is connected to the second one (2) just at Γ. This unusual behavior can be understood from the electronic structure of individual Ge nanocrystals which, in the absence of SO coupling, is composed of two sets of sixfold-degenerate (including spin) states with S and P envelope wave functions. It is recalled that, in semiconductor nanocrystals, the eigenstates near band edges can be approximately written as products of periodic Bloch states (here of p character) by envelope wave functions (here of S or P character) [25]. For a nanocrystal diameter of 4.4 nm, the P level is about 10 meV below the S level. In superlattices, due to the coupling between neighbor nanocrystals, S and P bands are formed and their respective energy positions are shifted in such a manner that the bands shown in Fig. 4(a) are mainly the P ones.

The results of Fig. 4(a) are well described by a twelve-band effective tight-binding model in which each nanocrystal is treated as one site on a honeycomb lattice and in which there are three spin-degenerate P states per nanocrystal (Appendix A) [16,31,32]. We deduce from this effective model that bands 1–3 [Fig. 4(a)] are derived from the $P_{x,y}$ states where xy is the lattice plane. Band 1 is flat due to destructive interferences of electron hopping induced by the honeycomb geometry [31,32]. The two bands characterized by a Dirac cone at ∼0.38 eV are formed by the P_z states perpendicular to the lattice.

2. Superlattice band structure for weak SO coupling

When a small amount of SO coupling is introduced in the atomistic tight-binding calculation, e.g., 10% of the nominal value on each Ge atom [Fig. 4(b)], gaps are formed, at Γ between bands 1 and 2, and at the Dirac cones at K. The SO coupling also induces avoiding crossings between $P_{x,y}$ and P_z bands. Calculations of the Z_2 topological invariant show that the gaps between bands 1, 2, and 3 are nontrivial. Interestingly, topological gaps are found for even smaller percentages of the SO coupling. This can be explained as follows. Appendix A shows that band structures obtained using the atomistic approach are very well reproduced by the effective tight-binding model in which an effective SO coupling $\lambda \mathbf{L} \cdot \mathbf{S}$ is introduced. $\mathbf{L}$ ($\mathbf{S}$) is the P orbital (spin) angular momentum. λ does not coincide with its atomic value on Ge p orbitals but is an effective value influenced by the quantum confinement and band mixing. Recently, Zhang *et al.* [33] have performed a deep theoretical investigation of the model system of $P_{x,y}$ orbitals on a honeycomb lattice with SO coupling. In agreement with our findings, they demonstrate the nontrivial topology of the highest bands whatever the intensity of the SO coupling. The reason is that the gaps at Γ and K are entirely due to the SO interaction, at least in the absence of sublattice asymmetry, which is the case here.

3. Superlattice band structure for strong SO coupling

When the SO coupling is increased in the atomistic tight-binding calculation [50% in Fig. 4(c), 100% in Fig. 2(a)], the band structure is modified in such a manner that it cannot be described by the effective model. However, gaps remain between bands 1 and 2, as well as between bands 2 and 3. Therefore, when the SO coupling varies from 0% to 100% (excluding 0%), the topology of bands 1 and 2 is preserved.

4. Conclusions on the origin of the nontrivial topology

All these results show that the nontrivial topology of the bands in superlattices of Ge nanocrystals comes from the combined effect of three factors [15]: (1) the p character of Ge valence bands combined with the P character of nanocrystal envelope wave functions involved in the highest bands; (2) the honeycomb lattice giving situations where the minibands are in contact at single points, at K or Γ; (3) the opening of gaps at these points by the SO coupling encoded as an effective on-site term in the P sector [16,33]. Figures 2(c)–2(d) show that the width of the nontrivial gaps strongly depends on size and geometry. Indeed, the effective SO coupling (λ) results from the subtle mixing of the light-hole, heavy-hole, and split-off band states induced by the strong confinement in the honeycomb lattice [15].

Another consequence of the SO interaction is the Rashba effect [34] induced by a small asymmetry of the superlattices in the perpendicular direction (z) that coincides with the $\langle 111 \rangle$ axis of the zinc-blende crystal. This leads to a splitting of the levels which are otherwise twofold degenerate, for each $\mathbf{k}$ vector, except at Γ, K, and M [3,30]. However, this splitting is found to be very small, always below 1 meV.

Appendix B explains the formation of the band structure from another limit, when the nanocrystals are uncoupled but the SO coupling is considered. All these descriptions of the band structures in an effective tight-binding approach work well because the electronic waves of the highest valence bands (or lowest conduction bands) are strongly confined in Ge spheres (see Ref. [16] for CdSe). In contrast, the nearly free electron description of Ref. [15] applies when the honeycomb pattern is induced by a weak, slowly variable potential that can be treated in perturbation in a $\mathbf{k} \cdot \mathbf{p}$ framework.

An important prediction of the calculations is that the nontrivial gaps are much larger in Ge than in CdSe superlattices [16]. The lighter effective masses for holes in Ge imply enhanced confinement effects. Ge, characterized by remarkably light effective masses [21] and strong SO coupling in the valence band, is certainly one of the best conventional semiconductors to get strong TI effects using nanostructural engineering. Another interesting result is that band 2 [Fig. 2(a)] is quite flat for this type of honeycomb nanogeometry. Flat bands and nontrivial topology are key ingredients to realize the fractional QH effect [35,36].

IV. Ge/Si SUPERLATTICES

These inspiring results motivated the study of the second type of superlattices which could be made using Ge/Si nanotechnology. Results of atomistic tight-binding calculations are presented in Fig. 5. In all the investigated configurations, there is a well-defined nontrivial gap between the two highest bands (1 and 2), exactly like for superlattices of Ge nanocrystals. Once again, the nontrivial topology of the bands is confirmed by a unitary D and by the presence of helical edge states in the gaps of the ribbons. The second gap, between bands 2 and 3, has a nonzero width when the thickness t of the layer, i.e., the height of the cylinders, is small compared to the diameter d of the Ge cylinders. A typical example of band structure in this configuration is displayed in Fig. 5(a). In the opposite case ($t > d$), the band 2 becomes very dispersive and the second energy gap vanishes [Fig. 5(b)]. The variations of the gaps with d and t [Fig. 5(c) and Fig. 5(d), respectively] support this analysis.

The great similarity between the results obtained for the two types of superlattices suggests that there is some flexibility in the choice of the geometry of the Ge components, provided that the honeycomb lattice is defined and there is a sufficient coupling between neighbor Ge islands. It also shows that strains do not have an important influence on the topology of the bands if the gaps are preserved.

The width of the first gap is maximum when $t \approx d$ and tends to increase with decreasing size (Fig. 5). However, a

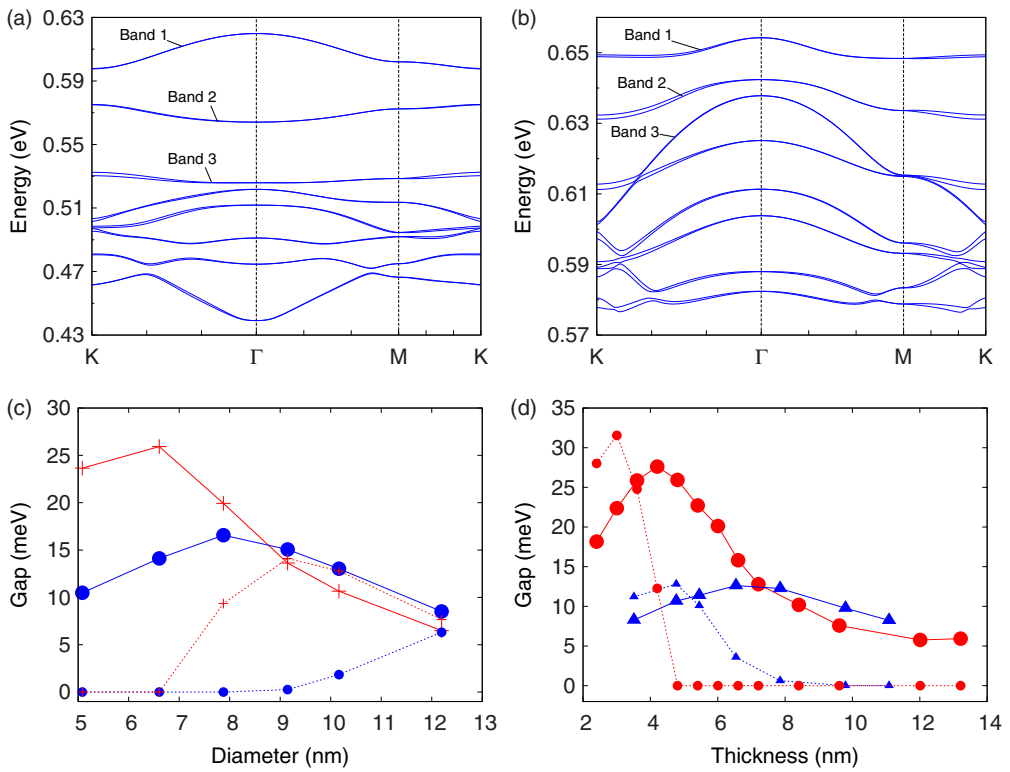

FIG. 5. (Color online) Results for Ge/Si superlattices as described in Fig. 1(b). (a) Highest valence bands for the superlattice characterized by $d = 1.1a = 6.6$ nm, $t = 3$ nm. (b) Same but for $t = 13.2$ nm. (c) Width of the nontrivial gaps as a function of the diameter d of the cylinders for $t = 4.8$ nm (+, red) and $t = 7.2$ nm (•, blue): gap between bands 1 and 2 (solid line), between bands 2 and 3 (dotted line). (d) Same but as a function of the thickness t of the sheet for $d = 6.6$ nm (•, red) and $d = 10.2$ nm (▲, blue).

nontrivial gap of ≈10 meV can be obtained using feature size of the order of 10 nm.

V. PROPOSITIONS FOR THE PRACTICAL REALIZATION OF THE STRUCTURES

The realization of ten-nanometer size patterns in Ge or Si using electronic lithography is challenging but possible. Honeycomb superlattices of Ge could be obtained by patterning thin Ge layers, for example using Ge-on-insulator technology [21,37–39]. In addition, considerable progress has been made in the formation of high-quality gate dielectrics on Ge to isolate the structures [21].

Another approach would be to use a Ge/Si technology, for example to start from a Si (or Si_xGe_{1-x}) sample, to pattern it, and to grow Ge in the cavities. Since Si and Ge have a lattice mismatch of 4.2%, the growth of defect-free 2D layers is problematic. However, the growth of nanostructured materials with lower dimensionality is much more favorable because the lattice misfit can be more easily accommodated due to the new boundary conditions [40], as shown for Si/Ge nanowires [41]. Another interesting approach would be to use the lateral epitaxial growth of Ge on Si/SiO_2 structures [42–44].

In order to observe the topological edge states using transport measurements, the positioning of the Fermi level in the first gap is required by filling the highest band with two holes per unit cell (four holes for the second gap). A main advantage of ordinary semiconductors is the ability to control the carrier concentration with a high precision, allowing for example to position the Fermi level between two Landau levels and to observe the QH effect (another topological state) [1,45].

Two holes per unit cell correspond to a density of $\approx 10^{18}$ cm^{-3} for $a = 10$ nm and $t = 7.2$ nm, easily achievable using electrostatic gating or doping [46]. Another possibility is to use modulation-doped superlattices, as already demonstrated for Ge quantum wells [47,48], for example starting from a doped Si (Si_xGe_{1-x}) layer. The generation of a hole density of 10^{18} cm^{-3} is also possible using optical pumping [49]. Finally, the edge states could be revealed using near-field microscopy approaches [50], avoiding the need to position the Fermi level in the gaps.

VI. CONCLUSION

In conclusion, it was shown that 2D TIs could be artificially fabricated using Ge or Ge/Si nanotechnology. Honeycomb superlattices of Ge with nanoscale geometry exhibit nontrivial gaps in the valence band due to the quantum confinement and the SO coupling. Ge/Si nanotechnology was already considered as a promising way to manipulate the spin of holes [51]. It should be a very interesting approach for the realization of spintronic devices exploiting TI properties.

ACKNOWLEDGMENTS

The author acknowledges very fruitful discussions with C. Morais Smith and D. Vanmaekelbergh.

APPENDIX A: HONEYCOMB LATTICE OF *p* ORBITALS WITH SPIN-ORBIT COUPLING

This section describes the twelve-band effective tight-binding model in which each nanocrystal of a superlattice is seen as an "artificial" atom, as one site on a honeycomb lattice. A similar model was investigated in depth in Ref. [33]. Figure 6 shows band structures calculated using this model including three P orbitals (P_x, P_y, P_z) per site and for each spin, P denoting the angular momentum of the envelope wave function. The on-site energies in the tight-binding Hamiltonian are E_{p_x} ($=E_{p_y}$) and E_{p_z}, that are not equal because the P_z states perpendicular to the lattice are not equivalent to the $P_{x,y}$ states. All hopping terms, i.e., nearest-neighbor interactions, can be written in the two-center approximation as functions of two parameters ($V_{pp\sigma}$, $V_{pp\pi}$) plus geometrical factors, following

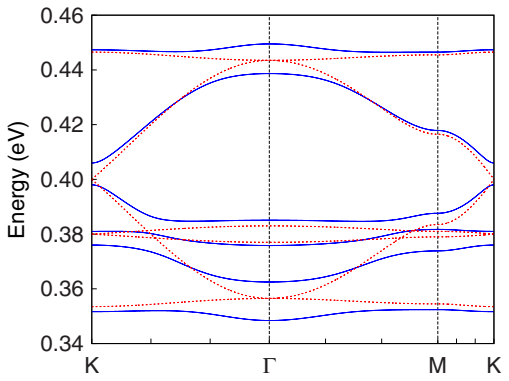

FIG. 6. (Color online) Band structure for a model of p orbitals on a honeycomb lattice with (blue solid line, $\lambda = 6$ meV) or without (red dotted line, $\lambda = 0$) SO coupling. Parameters: $E_{p_x} = E_{p_y} = 0.40$ eV, $E_{p_z} = 0.38$ eV, $V_{pp\sigma} = 30$ meV, $V_{pp\pi} = -1$ meV.

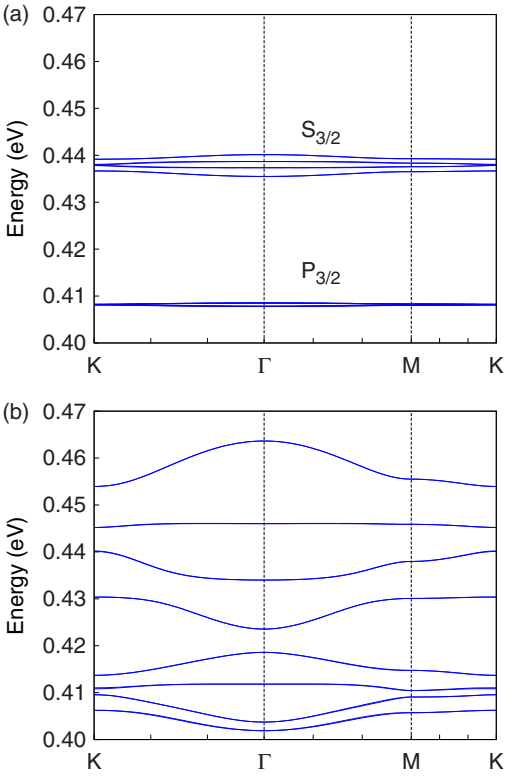

FIG. 7. (Color online) Highest valence bands calculated for superlattices of Ge nanocrystals ($d = a = 4.4$ nm), for $d_{cyl} = 0.05d$ (a) and $d_{cyl} = 0.2d$ (b).

Slater and Koster [52]. The SO interaction, written in the subspace of the P orbitals, leads to an effective coupling $\lambda \mathbf{L} \cdot \mathbf{S}$. The problem for the P_z bands is separable from the others in the absence of SO coupling.

The red dotted lines in Fig. 6 depict a band structure calculated with $\lambda = 0$. For reasonable values of the parameters, the model describes very well the highest minibands of Fig. 4(a) for a superlattice of Ge nanocrystals in the absence of SO coupling. The P_z bands, centered around a Dirac cone at 0.38 eV, are not very dispersive due to weak $pp\pi$ interactions. The other bands, derived from the $P_{x,y}$ states, exhibit another Dirac cone at 0.40 eV and two flat bands that touch the other bands just at Γ.

A nonzero effective SO coupling in the tight-binding model opens nontrivial gaps at Γ and K (blue solid lines in Fig. 6) [33]. It also couples P_z and $P_{x,y}$ bands, leading to avoiding crossings. The model explains the behavior of the highest minibands calculated using the atomistic approach [Fig. 4(b)] for weak SO coupling, confirming that the gaps are induced by the SO interaction and explaining the nontrivial topology of the bands.

There are differences between the band structures calculated using the atomistic tight-binding calculations (Fig. 4) and the effective model (Fig. 6) due to couplings with other bands that are not included in the model, such as S and D states. For the same reason, the model is not able to explain the band structure for larger values of the SO coupling [Fig. 4(c)] that induce complex mixing of the bands.

APPENDIX B: BAND STRUCTURES IN THE WEAK-COUPLING LIMIT

It is also instructive to look at the band structure of superlattices of Ge nanocrystals from another perspective. Figure 7(a) presents the highest minibands calculated for the same nanocrystals as in Fig. 2(a) but for a very small coupling between neighbor nanocrystals ($d_{\mathrm{cyl}} = 0.05d$). Two manifolds of four (twofold degenerate) bands are found at energies which coincide with the $S_{3/2}$ and $P_{3/2}$ levels predicted for the individual nanocrystals. These states can be roughly described as products of a p-like Bloch function with a total momentum $J = 3/2$ and an envelope wave function of S or P character, respectively.

When the coupling between neighbor nanocrystals is increased, for example for $d_{\mathrm{cyl}} = 0.2d$ [Fig. 7(b)], the width of the bands obviously increases. At the same time, gaps are formed between the bands and we recover a situation already close to the one found for $d_{\mathrm{cyl}} = 0.5d$ [Fig. 2(a)]. It nicely shows that the effective SO coupling, at the origin of the gaps, depends on the couplings between the nanocrystals.

[1] M. Z. Hasan and C. L. Kane, Rev. Mod. Phys. **82**, 3045 (2010).
[2] X.-L. Qi and S.-C. Zhang, Rev. Mod. Phys. **83**, 1057 (2011).
[3] C. L. Kane and E. J. Mele, Phys. Rev. Lett. **95**, 146802 (2005).
[4] A. H. Castro Neto, F. Guinea, N. M. R. Peres, K. S. Novoselov, and A. K. Geim, Rev. Mod. Phys. **81**, 109 (2009).
[5] B. A. Bernevig, T. L. Hughes, and S.-C. Zhang, Science **314**, 1757 (2006).
[6] M. König, S. Wiedmann, C. Brüne, A. Roth, H. Buhmann, L. W. Molenkamp, X.-L. Qi, and S.-C. Zhang, Science **318**, 766 (2007).
[7] T. Hirahara, G. Bihlmayer, Y. Sakamoto, M. Yamada, H. Miyazaki, S.-i. Kimura, S. Blügel, and S. Hasegawa, Phys. Rev. Lett. **107**, 166801 (2011).
[8] Y. Xu, B. Yan, H.-J. Zhang, J. Wang, G. Xu, P. Tang, W. Duan, and S.-C. Zhang, Phys. Rev. Lett. **111**, 136804 (2013).
[9] Y. Ohtsubo, P. Le Fèvre, F. Bertran, and A. Taleb-Ibrahimi, Phys. Rev. Lett. **111**, 216401 (2013).
[10] B. Singh, H. Lin, R. Prasad, and A. Bansil, Phys. Rev. B **88**, 195147 (2013).
[11] C.-C. Liu, W. Feng, and Y. Yao, Phys. Rev. Lett. **107**, 076802 (2011).
[12] D. Zhang, W. Lou, M. Miao, S.-C. Zhang, and K. Chang, Phys. Rev. Lett. **111**, 156402 (2013).
[13] C. Liu, T. L. Hughes, X.-L. Qi, K. Wang, and S.-C. Zhang, Phys. Rev. Lett. **100**, 236601 (2008).
[14] I. Knez and R.-R. Du, Front. Phys. **7**, 200 (2011).
[15] O. P. Sushkov and A. H. Castro Neto, Phys. Rev. Lett. **110**, 186601 (2013).
[16] E. Kalesaki, C. Delerue, C. Morais Smith, W. Beugeling, G. Allan, and D. Vanmaekelbergh, Phys. Rev. X **4**, 011010 (2014).
[17] C. Brüne, A. Roth, H. Buhmann, E. M. Hankiewicz, L. W. Molenkamp, J. Maciejko, X.-L. Qi, and S.-C. Zhang, Nat. Phys. **8**, 486 (2012).
[18] C.-H. Park and S. G. Louie, Nano Lett. **9**, 1793 (2009).
[19] M. Gibertini, A. Singha, V. Pellegrini, M. Polini, G. Vignale, A. Pinczuk, L. N. Pfeiffer, and K. W. West, Phys. Rev. B **79**, 241406 (2009).
[20] L. Fu and C. L. Kane, Phys. Rev. B **74**, 195312 (2006).
[21] R. Pillarisetty, Nature (London) **479**, 324 (2011).
[22] P. N. Keating, Phys. Rev. **145**, 637 (1966).
[23] Y. M. Niquet, D. Rideau, C. Tavernier, H. Jaouen, and X. Blase, Phys. Rev. B **79**, 245201 (2009).
[24] D. J. Chadi, Phys. Rev. B **16**, 790 (1977).
[25] C. Delerue and M. Lannoo, *Nanostructures–Theory and Modelling* (Springer, New York, 2004).
[26] E. Kalesaki, W. H. Evers, G. Allan, D. Vanmaekelbergh, and C. Delerue, Phys. Rev. B **88**, 115431 (2013).
[27] C. Delerue, Phys. Chem. Chem. Phys. (2014), doi:10.1039/C4CP01878H.
[28] Y. M. Niquet, C. Delerue, G. Allan, and M. Lannoo, Phys. Rev. B **62**, 5109 (2000).
[29] T. Fukui and Y. Hatsugai, J. Phys. Soc. Jpn. **76**, 053702 (2007).
[30] W. Beugeling, N. Goldman, and C. M. Smith, Phys. Rev. B **86**, 075118 (2012).
[31] C. Wu, D. Bergman, L. Balents, and S. Das Sarma, Phys. Rev. Lett. **99**, 070401 (2007).
[32] K. Sun, Z. Gu, H. Katsura, and S. Das Sarma, Phys. Rev. Lett. **106**, 236803 (2011).
[33] G.-F. Zhang, Y. Li, and C. Wu, Phys. Rev. B **90**, 075114 (2014).

[34] E. Rashba and E. Sherman, Phys. Lett. A **129**, 175 (1988).
[35] M. Goerbig, Eur. Phys. J. B **85**, 1 (2012).
[36] W. Beugeling, E. Kalesaki, C. Delerue, Y. Niquet, D. Vanmaekelbergh, and C. Morais Smith (unpublished).
[37] L. Hutin, C. Le Royer, J.-F. Damlencourt, J.-M. Hartmann, H. Grampeix, V. Mazzocchi, C. Tabone, B. Previtali, A. Pouydebasque, M. Vinet, and O. Faynot, IEEE Electron Device Lett. **31**, 234 (2010).
[38] D. D. Zhao, T. Nishimura, C. H. Lee, K. Nagashio, K. Kita, and A. Toriumi, Appl. Phys. Express **4**, 031302 (2011).
[39] B. Liu, X. Gong, C. Zhan, G. Han, H.-C. Chin, M.-L. Ling, J. Li, Y. Liu, J. Hu, N. Daval, C. Veytizou, D. Delprat, B.-Y. Nguyen, and Y.-C. Yeo, IEEE T. Electron Dev. **60**, 1852 (2013).
[40] P. Caroff, M. E. Messing, B. M. Borg, K. A. Dick, K. Deppert, and L.-E. Wernersson, Nanotechnology **20**, 495606 (2009).
[41] M. Amato, M. Palummo, R. Rurali, and S. Ossicini, Chem. Rev. **114**, 1371 (2014).
[42] V. D. Cammilleri, V. Yam, F. Fossard, C. Renard, D. Bouchier, P. F. Fazzini, L. Ortolani, F. Houdellier, and M. Hÿtch, Appl. Phys. Lett. **93**, 043110 (2008).
[43] H.-Y. Yu, S.-l. Cheng, J.-H. Park, A. K. Okyay, M. C. Onbal, B. Ercan, Y. Nishi, and K. C. Saraswat, Appl. Phys. Lett. **97**, 063503 (2010).
[44] K. Toko, Y. Ohta, T. Sakane, T. Sadoh, I. Mizushima, and M. Miyao, Appl. Phys. Lett. **98**, 042101 (2011).
[45] K. Klitzing, G. Dorda, and M. Pepper, Phys. Rev. Lett. **45**, 494 (1980).
[46] T. Ando, A. B. Fowler, and F. Stern, Rev. Mod. Phys. **54**, 437 (1982).
[47] H. v. Känel, M. Kummer, G. Isella, E. Müller, and T. Hackbarth, Appl. Phys. Lett. **80**, 2922 (2002).
[48] B. Rössner, G. Isella, and H. v. Känel, Appl. Phys. Lett. **82**, 754 (2003).
[49] N. Pauc, V. Calvo, J. Eymery, F. Fournel, and N. Magnea, Phys. Rev. Lett. **92**, 236802 (2004).
[50] C. Durand, M. Berthe, Y. Makoudi, J.-P. Nys, R. Leturcq, P. Caroff, and B. Grandidier, Nanotechnology **24**, 275706 (2013).
[51] C. Kloeffel, M. Trif, and D. Loss, Phys. Rev. B **84**, 195314 (2011).
[52] J. C. Slater and G. F. Koster, Phys. Rev. **94**, 1498 (1954).